Journal of Materials Science: Materials in Electronics (2019) 30:19035–19042
https://doi.org/10.1007/s10854-019-02261-5

Electrical transport and magnetoresistive properties of Nd-doped $La_{0.8}Sr_{0.2}MnO_3$ ceramics

Xiaojin Wang[1] · Qingming Chen[1] · Ling Li[1] · Chengyi Wang[1] · Peng Sun[1] · Hui Zhang[1]

Received: 4 June 2019 / Accepted: 23 September 2019 / Published online: 26 September 2019

Abstract
In this paper, $La_{0.8-x}Nd_xSr_{0.2}MnO_3$ ($x = 0.03$, 0.04, 0.05, and 0.06) ceramics were synthesized by a sol–gel method. The structure, surface morphology, electrical transport, and magnetoresistive properties of these materials were studied. X-ray diffraction (XRD) revealed samples to be single-phase with a distorted perovskite structure belonged to the ($R\bar{3}c$) space group. Scanning electron microscopy (SEM) revealed the samples to contain compact grains, with the grain size increasing slightly with the amount of doping Nd^{3+}. The standard four-probe method was used to test the electrical resistivity of the samples as a function of temperature (ρ–T). The metal–insulator transition temperature (T_p) shifted to lower temperatures and the resistivity (ρ) increased with the content of Nd^{3+}. Peak temperature coefficient of resistance (*TCR*) and magnetoresistance (*MR*) were both affected by the Nd^{3+} substitution. At $x = 0.05$, peak *TCR* and *MR* reached 5.12% K^{-1} and 19.78%, respectively. The mechanism responsible for both electrical and magnetoresistive properties of these materials was discussed in the frame of double-exchange (DE) interaction.

1 Introduction

In the 1950s, Zener proposed the double exchange (DE) mechanism to explain the coexistence of ferromagnetic and metallic states in doped perovskite manganites [1]. This mechanism involves two electrons on the adjacent Mn^{3+} and Mn^{4+} ions to simultaneously hop through the bridge O^{2-} ion such that the system had minimum energy only when the spin of the itinerant electron was oriented with the core spin of the Mn ion. In the 1960s, Nagaev predicted a potential phase separation mechanism in magnetic semiconductors by which transporting electrons can be separated from the antiferromagnetic background, with the ferromagnetic region being stabilized via localization effect of the itinerant electrons. In 1975, this prediction was proved in a ferromagnetic semiconductor. In 1995, Millis carried out a systematic study on $La_{1-x}Sr_xMnO_3$ [2], and the results revealed that the DE model failed to explain the ferroelectric properties of manganites. The electron–phonon Jahn–Teller effect and the influence of magnetic polarization were considered later, and this was very important to interpret the electrical and magnetic transport properties involve in the magnetoresistive behavior of manganites. Despite these advances, many experimental results still remain unexplained namely, the appearance of paramagnetic metal and ferromagnetic insulating phases after Mn-site ions doping and the Curie temperature (T_c) being much higher than the metal–insulator transition temperature (T_p). These experimental results can be well explained by the phase separation theory [3].

Doped-perovskite manganites with the general formula $T_{1-x}D_xMnO_3$ (T: trivalent rare earth elements such as La^{3+}, Nd^{3+}, Sm^{3+}; D: divalent alkali earth element such as Ca^{2+}, Sr^{2+}, Ba^{2+}) have been extensively studied in the past decades owing to their unique electrical and magnetic behavior including the existence of phase separation, charge/orbital ordering, colossal magnetoresistance (CMR), ferromagnetic–paramagnetic (FM–PM) transition, and metal–insulator (M–I) transition [4–12]. This behavior can be explained based on a DE interaction and the Jahn–Teller effect [13–15].

The microstructure, grain size, chemical uniformity, and preparation method of ceramics has a significant influence on their electromagnetic properties [16]. The most common way to prepare polycrystalline ceramic samples is by the conventional solid-state reaction. This method requires long sintering times, high temperatures, and several intermediate grinding steps to obtain the desired compound with

✉ Hui Zhang
harry_zhang71@163.com

[1] Faculty of Materials Science and Engineering, Kunming University of Science and Technology, Kunming 650093, Yunnan, China

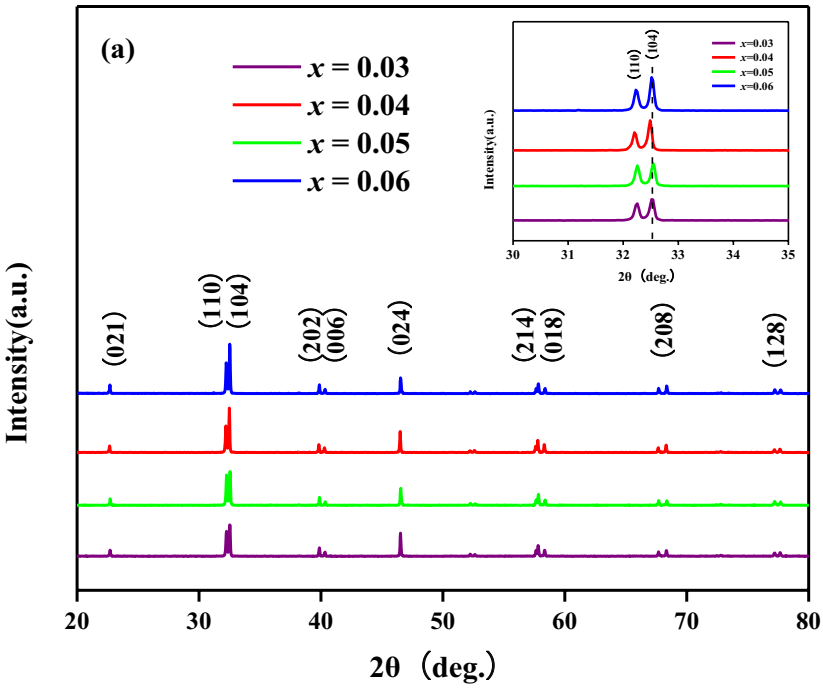
(a)
x = 0.03
x = 0.04
x = 0.05
x = 0.06
Intensity(a.u.)
(021)
(110)
(104)
(202)
(006)
(024)
(214)
(018)
(208)
(128)
2θ (deg.)

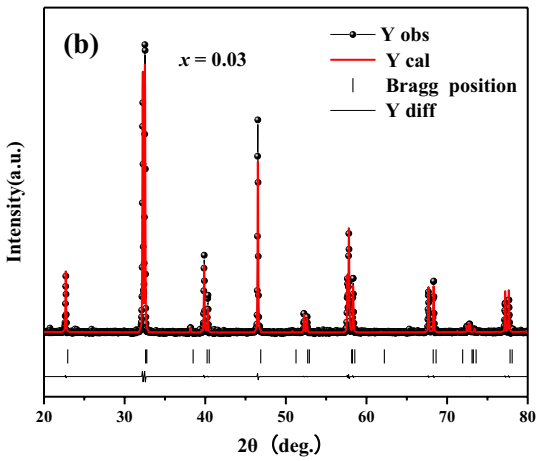
(b)
x = 0.03
Y obs
Y cal
Bragg position
Y diff
Intensity(a.u.)
2θ (deg.)

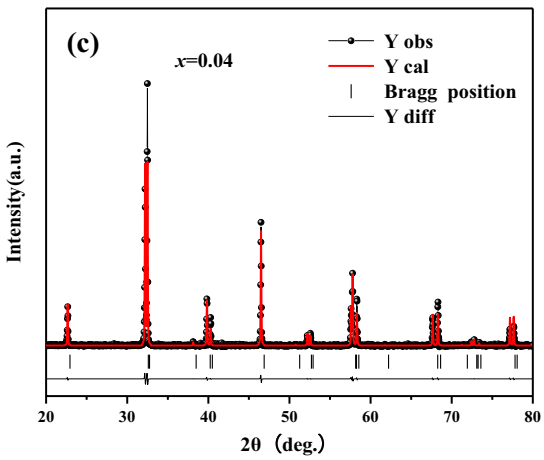
(c)
x=0.04
Y obs
Y cal
Bragg position
Y diff
Intensity(a.u.)
2θ (deg.)

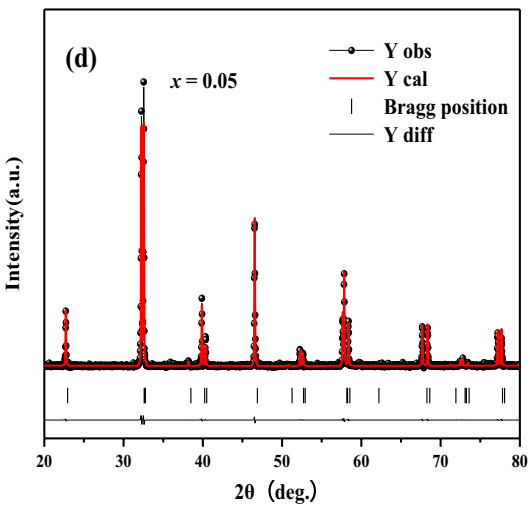
(d)
x = 0.05
Y obs
Y cal
Bragg position
Y diff
Intensity(a.u.)
2θ (deg.)

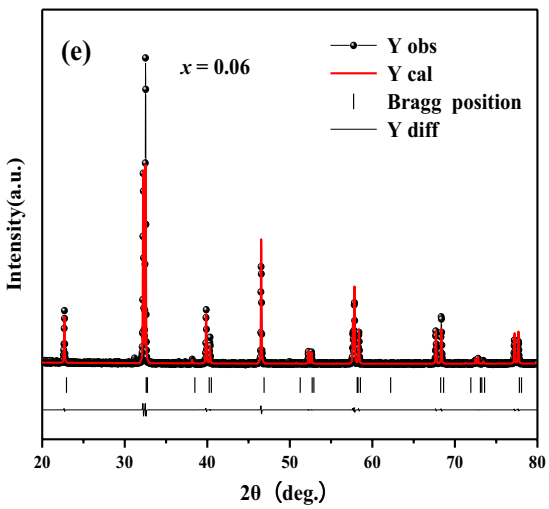
(e)
x = 0.06
Y obs
Y cal
Bragg position
Y diff
Intensity(a.u.)
2θ (deg.)

◂**Fig. 1** **a** XRD patterns of the LNSMO samples. **b–e** Rietveld refinement plots of typical $La_{0.8-x}Nd_xSr_{0.2}MnO_3$ ($x=0.03$, 0.04, 0.05, and 0.06) samples

homogenous composition. Co-precipitation requires solutions to be pH adjusted and aged for long times. Therefore, these methods are costly and complex. Comparatively, the sol–gel method has attracted significant attention in last decade owing to its unique advantages including short preparation times and good doping uniformity [17–21].

Doping A-site ions with different valent ions changes the Mn^{3+}/Mn^{4+} ratio and the length and angle of the Mn–O–Mn bond, thus altering DE interaction and physical properties of manganites. According to the previous results [22–24], doping Mg^{2+}, Ca^{2+}, Ba^{2+}, Nd^{3+}, Bi^{3+} and other metallic elements changed some physical properties of $La_xSr_{1-x}MnO_3$ (LSMO) and $La_xCa_{1-x}MnO_3$ (LCMO) such as T_p and temperature coefficient of resistance (*TCR*) [25]. Remarkably, doping with Nd^{3+} resulted in LSMO with lower T_p and higher *TCR* values. The replacement of La^{3+} with Nd^{3+} decreases the A-site average cationic radius $< r_A >$ and the tolerance factor , thus suppressing the DE interaction. As a result, T_p is reduced and *TCR* is increased, as in the case of Ca^{2+} substituting for Sr^{2+} in LSMO. In addition, since Nd has good magnetic conductivity, it is interesting to study Nd-doped LSMO in terms of magnetic properties. In this paper, the electrical and magnetic properties of $La_{0.8-x}Nd_xSr_{0.2}MnO_3$ (LNSMO) ceramics prepared by a sol–gel method were systematically studied. These characteristics changed significantly with the amount of doping Nd^{3+}. The results revealed all the ceramics to be single-phase (hexagonal), with the grain size increasing with the Nd^{3+} content. The resistivity of the ceramic samples showed the same behavior under an external magnetic field of 1T, and these resistivity values were lower than those obtained in the absence of magnetic field. *TCR* and *MR* showed maximum values for a Nd^{3+} doping loading of 0.05. The electromagnetic transmission characteristics of the LNSMO ceramics can shed light to better understand the CMR mechanism of these materials. These properties can provide these materials with a wide range of technological applications in the field of magnetic recording media, magnetic sensors, magneto-electric devices, random access memory, and hard disk read heads [26].

2 Experiments

A series of $La_{0.8-x}Nd_xSr_{0.2}MnO_3$ ($x=0.03$, 0.04, 0.05, and 0.06) ceramic samples were prepared by a sol–gel method. First, the desired stoichiometric amounts of the precursors ($La(NO_3)_3{\cdot}nH_2O$, $Ca(NO_3)_2{\cdot}4H_2O$, $Mn(NO_3)_2{\cdot}4H_2O$, and $SrCl_2{\cdot}6H_2O$) were weighted and dissolved in methyl alcohol. Citric acid (molar ratio to metal ions of 4:1) and ethylene glycol (ca. 40 mL) were added to the mixed solution as chelating and gelification agents, respectively. The resulting solution was magnetically stirred on a hot plate at 80 °C for about 30 min and then it turned into faint yellow. The solution was slowly evaporated to become highly viscous, after which an orange transparent gel was formed. A xerogel was formed by drying the gel in an oven at 140 °C for 12 h. Second, the xerogel was ground into powder and calcined in air at 500 °C for 8 h. Finally, the calcined powders were ground again, pressed into pellets, and then sintered at 1450 °C for 12 h to obtain the bulk polycrystalline ceramic samples.

The structure and crystallinity of the LNSMO ceramic samples were examined by powder X-ray diffraction (XRD) on a device with Cu Kα radiation at room temperature. The surface morphologies and microstructures of the ceramic samples were characterized and analyzed by scanning electron microscopy (SEM). The resistivity of the ceramic samples were measured with the standard four probe method within a temperature range of 250–350 K. *MR* was measured under a magnetic field of 1 T using an ET9000 electrical transport property test system (ET9000, East Changing Technologies, Inc).

3 Results and discussion

3.1 Crystal structure and surface morphology

Figure 1a shows the XRD patterns of $La_{0.8-x}Nd_xSr_{0.2}MnO_3$ ($x=0.03$, 0.04, 0.05, and 0.06) from 20º to 80º. As shown in Fig. 1a, the room-temperature patterns of the ceramic samples contained sharp diffraction peaks, and no other heterogeneous phases were detected within the sensitivity of the instrument. Thus, the polycrystalline ceramic samples showed good crystallinity. All samples showed patterns typical of perovskite structure (PDF card 51-0409) that belonged to the hexagonal crystal system and the space group ($R\bar{3}c$). The inset in Fig. 1a represents a magnified view of the diffraction peaks corresponding to the planes (110) and (104). The most intense peaks did not shift significantly with the amount of doping Nd, which might be due to the little change of cell volume [27].

The XRD Rietveld results are illustrated in Fig. 1b–e. The solid spheres are the diffraction data and the red line represents the fitting result. The short vertical line is the fitting diffraction peak position, while the bottom solid line is the difference between the measured and the fitting values. The experimental diffraction peaks were consistent with those of the XRD Rietveld, further proving that all samples were single-phase crystallized.

Table 1 displays the structural parameters and refinement parameters of all samples. The samples showed a hexagonal

Table 1 The structure parameters and refinement parameters of LNSMO samples

γ (mol%)		3	4	5	6
Space group		$R\bar{3}c$	$R\bar{3}c$	$R\bar{3}c$	$R\bar{3}c$
Lattice constant (Å)	a	5.52093	5.51900	5.52104	5.51810
	b	5.52093	5.51900	5.52104	5.51810
	c	13.35760	13.35270	13.35170	13.34630
Cell volume (Å^3)	V	352.6010	352.2253	352.4593	351.9416
Bond distance (Å)	Mn–Mn	3.88799	3.88661	3.88748	3.88557
	Mn–O	1.96281	1.96211	1.96255	1.96159
Bond angles (°)	Mn–O–Mn	164.1233	164.1232	164.1218	164.1216
Fit index (%)	R_e	7.47014	7.25398	7.08562	7.07443
	R_b	7.86075	9.03198	7.03872	9.00948
	R_p	6.09518	6.7142	5.40477	6.40682
	χ	1.10731	1.55029	0.98681	1.62187

perovskite structure and ($R\bar{3}c$) space group. All samples showed goodness of fitting (χ) values close to 1, revealing the feasibility of the fitted model. The length and angle of the Mn–O bond decreased with the amount of Nd^{3+} doped such that DE interaction between Mn^{3+}/Mn^{4+} in the MnO_6 octahedron [28–31] decreased, showing a great impact on the electrical performance of the polycrystalline ceramic samples. Considering the ionic radii of La^{3+} (1.216 Å) and Nd^{3+} (1.163 Å), the total ionic radius and the cell volume both decreased upon substitution of La^{3+} with Nd^{3+}. However, due to the close ionic radius of La^{3+} and Nd^{3+} and the low doping amount, the volume of the unit cell only decreased slightly.

Figure 2a–d shows the surface morphology of the $La_{0.8-x}Nd_xSr_{0.2}MnO_3$ ($x = 0.03$, 0.04, 0.05, and 0.06) polycrystalline ceramic samples as observed by SEM. Pores were hardly observed because of the low amount of grain boundaries and other internal defects of the ceramic samples, which essentially reflects the intrinsic behavior of the electric properties. With the aim to further analyze the microstructure of LNSMO polycrystalline ceramics, Nano Measurer 1.2 was used to determine the grain size of the samples. As shown in Fig. 2e, the grain size increased slightly with the Nd^{3+} content, although this variation was very limited.

3.2 Electrical properties

Figure 3a and b shows the electrical resistivity as a function of temperature (ρ-T) within 250–350 K for $La_{0.8-x}Nd_xSr_{0.2}MnO_3$ ($x = 0.03$, 0.04, 0.05, and 0.06) ceramics for magnetic fields of 0 and 1 T, respectively. As can be seen in Fig. 3a, b, as the temperature increased, all samples underwent metal–insulator transformation at T_P within the temperature range studied herein. Insulators conduct electricity at high temperatures, while metals conduct electricity at low temperatures. T_P shifted towards lower temperatures and the electrical resistivity increased continuously with the loading of Nd^{3+}.

T_p decreased from 340.55 K to 329.42 K at 0 T (from 343.61 K to 336.28 K at 1 T) as the amount of Nd^{3+} increased from 0.03 to 0.06. The decrease of T_p with the amount of Nd^{3+} can be explained as follows. The Mn–O bond distance and angle both decreased with the amount of Nd^{3+}, thereby weakening the DE interaction between Mn^{3+}/Mn^{4+} in MnO_6 octahedron. As a result, the electron bandwidth decreased, which had a great impact on the electrical performance of the polycrystalline ceramic samples.

TCR can be defined by Eq. (1) as follows:

$$TCR\ (\%) = \left(\frac{1}{\rho} \times \frac{d\rho}{dT}\right) \times 100\% \quad (1)$$

where ρ and T are the resistivity and temperature, respectively.

Figure 4 shows the dependence of *TCR* with temperature (295–335 K) for the LNSMO ceramics. The inset in Fig. 4 shows the variation of peak *TCR* temperature (T_k) with the amount of dopant. T_k varied with the amount of dopant as T_p did. The substitution of larger La^{3+} with Nd^{3+} reduced the ionic radius, thus decreasing the Mn–O–Mn bond angle and weakening the DE interaction between Mn^{3+}/Mn^{4+}, which in turn resulted in lower T_k values. As the amount of Nd^{3+} increased, peak *TCR* showed a maximum at a certain Nd loading and decreased thereafter. When $x = 0.05$, peak *TCR* reached 5.12% K^{-1}. This value was higher than previous *TCR* values reported for $La_{0.845}Sr_{0.155}MnO_3$ and $La_{0.7}Sr_{0.3}MnO_3$ (2.33% K^{-1} [32] and 1.8% K^{-1} [33], respectively). Equation (1) reveals that the resistivity affects peak *TCR* value. The preparation method, sintering time, sintering temperature, sintering sample density, ionic radius, and other factors can also affect *TCR* [34, 35]. The resistivity and ionic radius are the

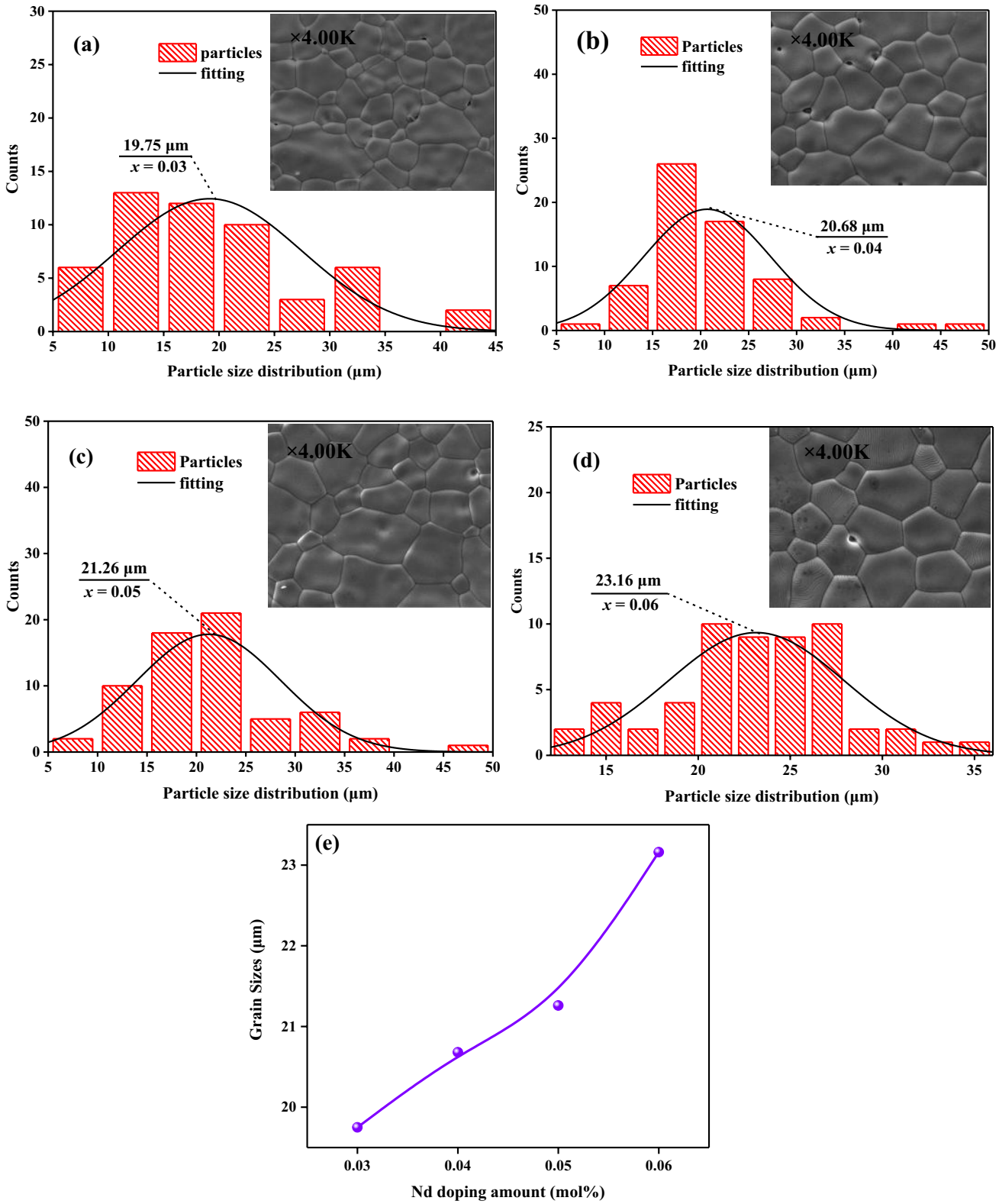

Fig. 2 **a**–**d** SEM images of the LNSMO samples with $x = 0.03$ (**a**), 0.04 (**b**), 0.05 (**c**), and 0.06 (**d**). **e** Variation trend of the grain size

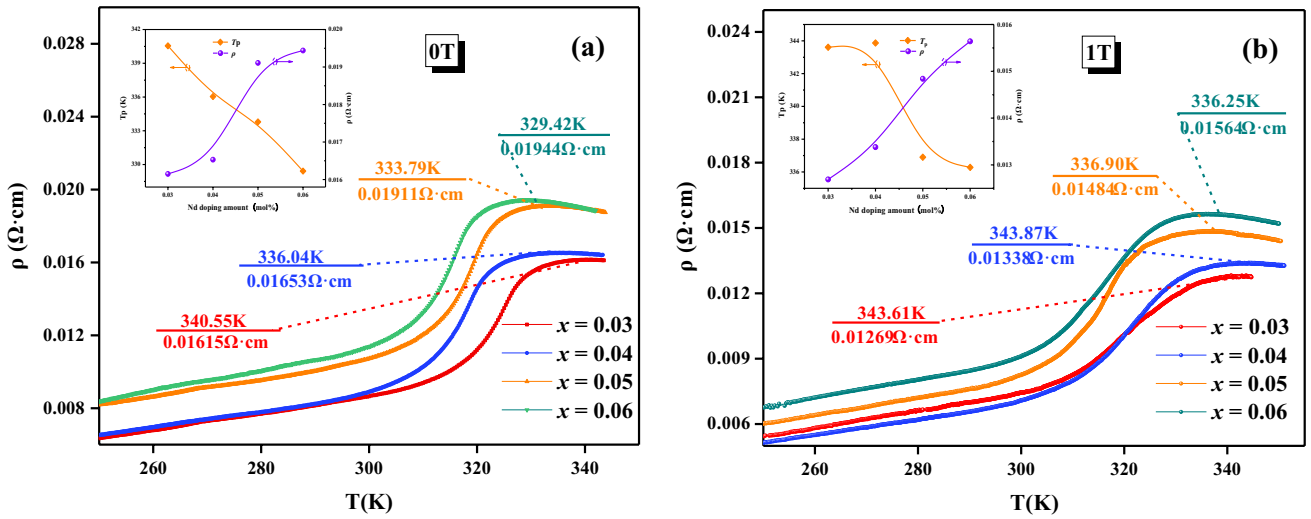

Fig. 3 Resistivity versus temperature plots of the LNSMO samples under different environmental conditions: **a** 0 T and **b** 1 T

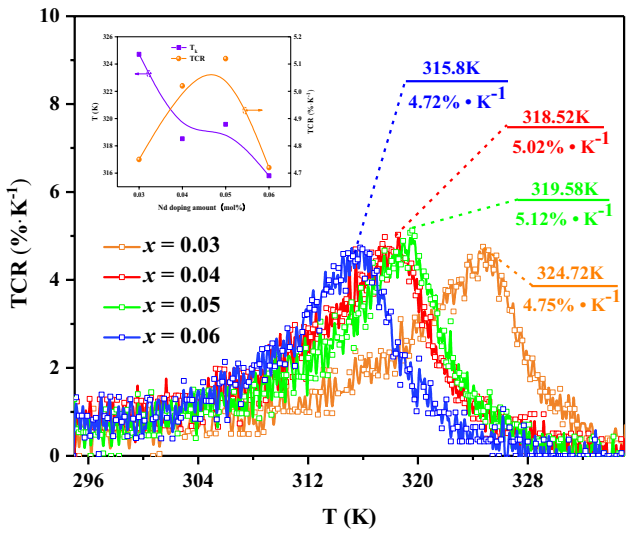

Fig. 4 *TCR* versus temperature plots for the LNSMO samples

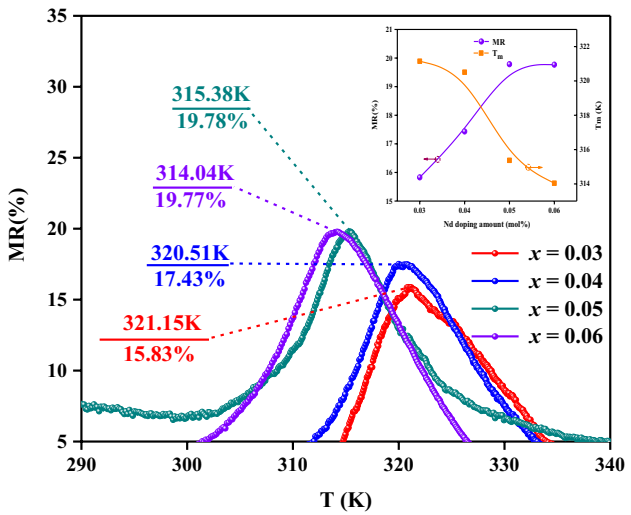

Fig. 5 *MR* versus temperature plots of the LNSMO samples

most important factors affecting peak *TCR*. At low Nd^{3+} loadings, peak *TCR* is mainly affected by the ionic radius, while the resistivity has little influence on peak *TCR*. However, when the doping amount reaches a certain level, the resistivity prevails and the ionic radius has little impact on peak *TCR*. At this point, the resistivity increases and peak *TCR* decreases with the amount of Nd^{3+}.

3.3 Magnetic properties

By comparing Fig. 3a and b, it can be seen that the samples showed lower resistivity when exposed to a magnetic field of 1 T. The magnetic field generated carrier delocalization, which inhibited the resistivity and increased the metal phase fraction as a result [36].

Figure 5 shows the variation of *MR* with temperature (290–340 K) for the LNSMO ($x = 0.03$, 0.04, 0.05, and 0.06) ceramics. The inset in Fig. 5 describes the change of peak *MR* temperature (T_m) and peak *MR*, with *MR* being defined by Eq. (2) as follows:

$$MR(\%) = \frac{\rho_0 - \rho_H}{\rho_0} \times 100\% \quad (2)$$

Peak *MR* temperature (T_m) changed similarly with temperature than T_p and T_k. La^{3+} was replaced by Nd^{3+}, and the ionic radius decreased, thus reducing the Mn–O–Mn bond

angle and the DE interaction between Mn^{3+}/Mn^{4+}, which in turn resulted in lower T_m values. *MR* showed a maximum at a certain Nd^{3+} loading and decreased thereafter, which is basically consistent with the trend of *TCR*. At $x = 0.05$, peak *MR* reached the maximum value (19.78%), with this value being higher than peak *MR* of $La_{0.8}Sr_{0.2}MnO_3$ (17.2%) [37]. Although Eq. (2) indicates that the resistivity affects *MR*, Nd has a good permeability, which improved the order of the grain magnetic domains. At low Nd^{3+} contents, peak *MR* increased as the order degree of the magnetic domains was higher. At high Nd^{3+} contents, the resistivity dominated. At this point, peak *MR* decreased slightly with the amount of Nd^{3+}.

4 Conclusions

LNSMO polycrystalline ceramics were prepared by a sol–gel method. The effects of the Nd^{3+} content on the structure, surface morphology, and electromagnetic transmission characteristics were studied and discussed. The XRD results revealed all the ceramics to be single-phased (hexagonal). SEM revealed that the grain size increased with the Nd^{3+} content. T_p, T_k, T_m, and the resistivity of the ceramic samples gradually decreased with the Nd^{3+} content. The resistivity of the ceramic samples behaved similarly under an external magnetic field of 1 T, although lower values were obtained compared to those obtained at 0 T. When the Nd^{3+} doping amount was 0.05, *TCR* and *MR* reached a maxima of 5.12% K^{-1} and 19.78%, respectively. Peak *TCR* and *MR* values obtained herein were slightly higher than those reported in the literature. Although the promotion effect was limited, the results indicated that a small amount of Nd^{3+} had a positive effect on the electrical transport and magnetoresistive properties of $La_{0.8}Sr_{0.2}MnO_3$ ceramics. These properties could be explained in terms of a DE interaction.

Acknowledgements This work was financially supported by the National Natural Science Foundation of China (Grant No. 11564021), the Analysis and Testing Foundation of Kunming University of Science and Technology, and the Innovation Training Program for College Students (Grant No. 201710674053).

References

1. C. Zener, Interaction between the *d*-Shells in the transition metals ferromagnetic compounds of manganese with perovskite structure. J. Phys. Rev. **82**, 403–405 (1951)
2. A.J. Millis, P.B. Littlewood, B.I. Shraiman, Double exchange alone does not explain the resistivity of $La_{1-x}Sr_xMnO_3$. Phys. Rev. Lett. **74**, 5144–5147 (1995)
3. J. Goodenough, Colossal magnetoresistance in $Ln_{1-x}A_xMnO_3$ perovskites. Aust. J. Phys. **52**, 155–186 (1999)
4. A.M. Haghirigosnet, J.P. Renard, CMR manganites: physics, thin films and devices. J. Phys. D **36**, R127 (2003)
5. J.B. Goodenough, Electronic structure of CMR manganites (invited). J. Appl. Phys. **81**, 5330–5335 (1997)
6. T.V. Ramakrishnan, Modelling colossal magnetoresistance manganites. J. Phys. **19**, 497–503 (2007)
7. R. Tripathi, V.P.S. Awana, H. Kishan, G.L. Bhalla, Search for room temperature high-*TCR* manganite/silver composites. J. Magn. Magn. Mater. **320**, L89–L92 (2008)
8. G.D. Tang, Z.Z. Li, L. Ma, W.H. Qi, L.Q. Wu, X.S. Ge, G.H. Wu, F.X. Hu, Three models of magnetic ordering in typical magnetic materials. Phys. Rep. **758**, 1–56 (2018)
9. J.J. Qian, W.H. Qi, Z.Z. Li, L. Ma, G.D. Tang, Y.N. Du, M.Y. Chen, G.H. Wu, F.X. Hu, Spin-dependent and spin-independent channels of electrical transport in perovskite manganites. RSC Adv. **8**, 4417–4425 (2018)
10. J.J. Qian, Z.Z. Li, W.H. Qi, L. Ma, G.D. Tang, Y.N. Du, M.Y. Chen, Study of magnetic structure and electrical-transport properties of $La_{1-y}Ba_yMn_{1-x}Fe_xO_3$ (y = 0.15, 0.40) perovskite manganites. J. Alloys Compd. **764**, 239–249 (2018)
11. D.G. Li, Y.T. Mai, J. Xiong, Y.H. Xiong, Z.L. Liu, C.S. Xiong, Studies on low-field and room-temperature magnetoresistance in $La_{2/3}(Ca_{1-x}Sr_x)_{1/3}MnO_3$ perovskites. J. Supercond. Novel Magn. **26**, 719–723 (2012)
12. T.D. Thanh, L.H. Nguyen, D.H. Manh, N.V. Chien, P.T. Phong, N.V. Khiem, L.V. Hong, N.X. Phuc, Structural, magnetic and magnetotransport behavior of $La_{0.7}Sr_xCa_{0.3-x}MnO_3$ compounds. Physica B **407**, 145–152 (2012)
13. C. Zener, Interaction between the d-shells in the transition metals. Phys. Rev. **81**, 440–444 (1951)
14. D.Y. Cao, Y.Y. Zhang, W.X. Dong, Structure, magnetic and transport properties of $La_{0.7}Ca_{0.3-x}Sr_xMnO_3$ thin films by sol-gel method. Ceram Int **41**, S381–S386 (2015)
15. H. Baaziz, A. Tozri, E. Dhahri, Effect of particle size reduction on the structural, magnetic properties and the spin excitations in ferromagnetic insulator La0.9Sr0.1MnO3 nanoparticles. Ceram Int **41**, 2955–2962 (2015)
16. J. Ma, Y. Cai, W. Wang, Q. Cui, M. Theingi, H. Zhang, Q. Chen, Enhancement of temperature coefficient of resistivity in $La_{0.67}Ca_{0.33}MnO_3$ polycrystalline ceramics. Ceram. Int. **40**, 4963–4968 (2014)
17. F. Jin, H. Zhang, X. Chen, X. Liu, Q. Chen, Improvement in electronic and magnetic transport of $La_{0.67}Ca_{0.33}MnO_3$ manganites by optimizing sintering temperature. J. Sol-Gel Sci. Technol. **81**, 1–8 (2016)
18. T. Sun, S. Zhao, F. Jin, X. Liu, Enhanced room-temperature *MR* and *TCR* in polycrystalline $La_{0.67}$ $(Ca_{0.33-x}Sr_x)MnO_3$ ceramics by oxygen assisted sintering. Ceram Int **44**, 2400–2406 (2018)
19. T. Sun, J. Jiang, Q. Chen, X. Liu, Improvement of room-temperature *TCR* and *MR* in polycrystalline $La_{0.67}(Ca_{0.27}Sr_{0.06})MnO_3$ ceramics by Ag_2O doping. Ceram. Int. **44**, 9865–9874 (2018)
20. I. Matos, S. Se´rio, Effect of the sintering temperature on the properties of nanocrystalline Ca1-xSmxMnO3 ($0 \le x \le 0.4$) powders. J. Alloys Compd. **509**, 9617–9626 (2011)
21. X. Yin, X. Liu, Y. Yan, Q. Chen, Preparation of $La_{0.67}Ca_{0.33}MnO_3$:Ag_x polycrystalline by sol-gel method. J. Sol-gel Sci. Technol. **70**, 361–365 (2014)
22. M.D. Daivajna, A. Rao, G.S. Okram, Electrical, thermal and magnetic studies on Bi-substituted LSMO manganites. J. Magn. Magn. Mater **388**, 90–95 (2015)
23. A. Sendil Kumar, K.R. Reddy, A.K. Bhatnagar, Magnetization and ESR studies of $La_{0.67}(Ca_{1-x}Mg_x)_{0.33}MnO_3$ systems. J. Alloys Compd. **639**, 139–144 (2015)
24. B. Munirathinam, M. Krishnaiah, S. Arumugam, M. ManivelRaja, Electronic transport and magnetic studies of $La_{1-x}Ca_{x-0.08}Sr_{0.04}Ba_{0.04}MnO_3$. J. Phys. Chem. Solids **71**, 1763–1767 (2010)

25. X. Chen, H. Zhang, F. Jin, X. Liu, Q.M. Chen, Fabrication of polycrystalline ceramics by sol-gel method. J. Sol-Gel Sci. Technol. **80**, 168–173 (2016)
26. P.M. Woodward, T. Vogt, D.E. Cox, Influence of cation size on the structural features of $Ln_{1/2}A_{1/2}MnO_3$ perovskites at room temperature. Chem. Mater. **10**, 3652–3665 (1998)
27. S. Zhao, X. Yue, X. Liu, Tuning room temperature T_p and *MR* of $La_{1-y}(Ca_{y-x}Sr_x)MnO_3$ polycrystalline ceramics by Sr doping. Ceram. Int. **43**, 4594–4598 (2017)
28. D.S. Fan, Q. Li, Y.M. Xuan, H. Tan, J.F. Fang, Temperature-dependent infrared properties of Ca doped (La, Sr) MnO_3 compositions with potential thermal control application. Appl. Therm. Eng. **51**, 255–261 (2013)
29. K.L. Yanapu, S.S. Samatham, D. Kumar, V. Ganesan, P.V. Reddy, Effect of bismuth doping on the physical properties of La-Li-Mn-O manganite. Appl. Phys. A **122**, 199 (2016)
30. J. Fontcuberta, B. Martínez, A. Seffar, S. Piñol, J.L. García-Muñoz, X. Obradors, Colossal magnetoresistance of ferromagnetic manganites: structural tuning and mechanisms. Phys. Rev. Lett. **76**, 1122–1125 (1996)
31. D.Y. Cao, Y.Y. Zhang, W.X. Dong, J. Yang, W. Bai, Y. Chen, G.S. Wang, X.L. Dong, X.D. Tang, Structure, magnetic and transport properties of thin films by sol-gel method. Ceram. Int. **41**, S381–S386 (2015)
32. G. Dong, T. Sun, F.Q. Ji, Y. Liu, S. Zhang, H. Zhang, X. Liu, Polycrystalline $La_{0.845}Sr_{0.155}MnO_3$:$Ag_x$ ceramics ($0 \le x \le 0.5$) with roomtemperature *TCR* and *MR* for improved uncooling photoelectric and magnetic devices. Ceram. Int. **45**, 12162–12168 (2019)
33. R. Tripathi, V.P.S. Awana, H. Kishan, G.L. Bhall, Search for room temperature high-*TCR* manganite/silver composites. J. Magn. Magn. Mater. **320**, L89–L92 (2008)
34. S. Das, T.K. Dey, Electrical conductivity and low field magnetoresistance in polycrystalline $La_{1-x}K_xMnO_3$ pellets prepared by pyrophoric method. Solid State Commun. **134**, 837–842 (2005)
35. G. Venkataiah, V. Prasad, P. Venugopal Reddy, Influence of A-site cation mismatch on structural, magnetic and electrical properties of lanthanum manganites. J Alloy Compd **429**, 1–9 (2007)
36. L. Li, H. Zhang, X. Liu, P. Sun, C.Y. Wang, X.J. Wang, B.B. Li, G.W. Liang, Q.M. Chen, Structure and electromagnetic properties of $La_{0.7}Ca_{0.3-x}K_xMnO_3$ polycrystalline ceramics. J. Ceram. Int. **45**, 10558–10564 (2019)
37. X.H. Yu, T. Sun, Q.M. Chen, Y.B. Duan, X. Liu, Modulation of room temperature *TCR* and *MR* in $La_{1-x}Sr_xMnO_3$ polycrystalline ceramics via Sr doping. J. Sol-Gel. Sci. Technol. **90**, 221–229 (2019)